Single-photon superradiance in waveguide-quantum-electrodynamical systems with whispering-gallery-mode resonators

Yao Zhou, Zihao Chen, and Jung-Tsung Shen

Phys. Rev. A **101**, 043831 — Published 23 April 2020

DOI: 10.1103/PhysRevA.101.043831

Single-photon superradiance in waveguide-QED systems with whispering-gallery-mode resonators

Yao Zhou, Zihao Chen, and Jung-Tsung Shen*

Department of Electrical and Systems Engineering,

Washington University in St. Louis,

St. Louis, MO 63130

Abstract

As a manifestation of cooperative interactions between a single photon and a cluster of atoms, single-photon superradiance has attracted considerable attention recently but has been studied insofar as that only quantum emitters are involved in the superradiance process. Here we expand the scope of investigation to study single-photon superradiance in a waveguide-QED system containing whispering-gallery-mode (WGM) resonators which are essential for many nano-photonic devices. It is shown analytically and numerically that single-photon superradiance can also occur when WGM resonators are present. The criteria for the emergence of the superradiant emission peak and the enhanced atom-light coupling strength are derived. Finally, the general case of a cascade of WGM resonators is investigated by a renormalization approach. Single-photon frequency comb generation is demonstrated via a frequency-modulated superradiant effective atom in chiral waveguide-QED systems with WGM resonators.

* jushen@wustl.edu

I. INTRODUCTION

Superradiance, the cooperative spontaneous emission between quantum emitters, was first discussed by Dicke in the system of a dense atom cloud [1]. It is a phenomenon due to the phase locking of the atomic dipoles throughout the medium, resulting in a cooperative emission process involving a collective mode of all the atoms of the sample [2]. In superradiance, atoms can spontaneously emit photons at a much higher decay rate than that of a single atom and the peak intensity of the emitted light scales as the square of the number of participating atoms, with a correspondingly narrowed temporal width [1]. Remarkably, the burst emission and the enhanced intensity can also occur when only one photon is stored in the atom cloud. Such a single-photon superradiance has recently attracted great attentions. It has been shown that the cooperative interaction in single-photon superradiance regime results in the collective Lamb shift [3, 4], the broadening of spectrum lineshape [5], and directed spontaneous emission [6]. These features offer potential applications for quantum control of spontaneous emission and ultrafast readout [7], and long-distance quantum communication with atomic ensembles [8].

Early work on single-photon superradiance primarily focused on the cases wherein atoms are in proximity with each other. Recently, single-photon superradiance is investigated for a spatially distributed system, where the distance between atoms are not negligible compared to photon wavelength [9–14]. On the other forefront, there has been an ever-increasing pace of activity in optical devices consisting of optical waveguides and whispering-gallery-mode (WGM) resonators (*e.g.*, micropost, microdisk, microsphere, microtoroid, and ring), which hold the promise of a new modality of light switching, amplification, and modulation [15, 16]. In both classical and quantum regimes, the solid-state WGM resonator-based photonic devices have been shown to enable several unique functionalities, such as add/drop filter for photon routing, slow light [17, 18], nano-particle sensing [19, 20], and scalable on-chip photonic qubit entanglement [21]. For distributed waveguide systems, it has been shown that single-photon multi-atom superradiance can be described by a single superradiant effective atom with a maximized superradiant decay rate [22]. It is of great interest to extend the single-photon superradiance phenomenon to functional configurations involving WGM resonators.

Superradiance, as the fundamental consequence of constructive phase interference of light

radiation paths, can take place in various systems involving the collective interaction between light and an ensemble of atoms. Several approaches have been developed to investigate the collectivity of some spatially extended atom ensembles, such as classical scattering approach [13] and atomic excitation eigenfunction approach [9]. In the classical scattering approach, the system dynamics are described by an effective Hamiltonian derived from master equations based on atomic density matrix. The atoms are treated as oscillating dipoles, where the atom-light interaction is characterized by classical scattering theory. Nevertheless it is fundamentally inadequate to apply a classical treatment in a photon Fock state system. The classical scattering approach features the consequent dependence of collective spontaneous decay rate on the geometry of an infinite atom lattice and sheds light on the behavior of a finite lattice general state at long times. The atomic excitation eigenfunction approach calculates the collective exponential decay rate of a dense atom cloud initially at single excitation state with specific atom density distribution. The single excitation of the system is described by a distribution function, with the collective decay rate of the atom cloud denoted by the eigenvalue of its time derivative. In density-operator treatment to describe an open quantum system, the degrees of freedom of the environment are traced out, and the resultant reduced density operator characterizes the subsystem of interest in terms of mixed states. Different from the density matrix treatment, our approach preserves the full quantum entanglement of the entire system throughout the interaction process; the subsystem of interest is then described in terms of restricted pure states and the dynamics governed by a non-Hermitian Hamiltonian. In our case, the non-Hermitian Hamiltonian describes the non-reciprocal photon leakage into the environment mode. Such a non-Hermitian Hamiltonian has also been adopted in recent works on the open quantum systems [23, 24].

In this article, Sec. II introduces the schematics of the system and the physical model describing the system dynamics. Sec. III and Sec. IV discuss the single-photon superradiance condition when multiple atoms couple to a single WGM resonator and when multiple atoms couple to a cascade of resonators, respectively. In Sec. V, an example of potential application of how ultra-strong superradiant coupling strength facilitates the generation of single-photon frequency comb is presented. Finally, in Sec. VI, we draw a conclusion and briefly discuss other potential applications regarding single-photon superradiance in WGM systems.

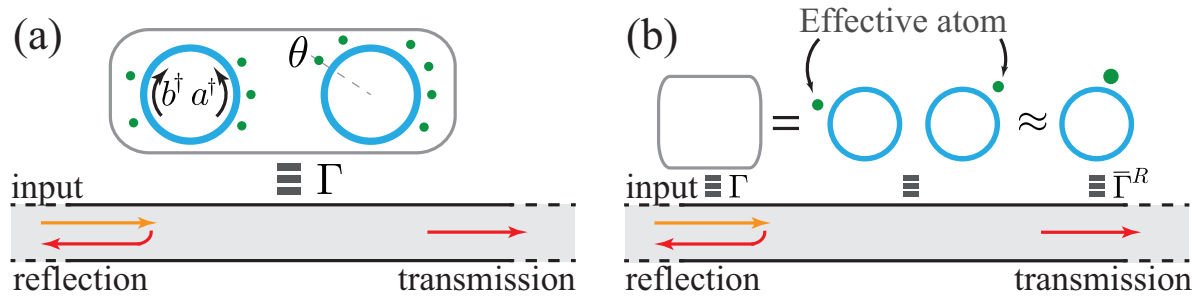

FIG. 1. (a) Distributed multi-resonator case. Shown is the case of two WGM resonators (blue rings). Each resonator couples with a number of two-level atoms (green dots). (b) Renormalization of the multi-resonator case: the atoms coupled to each resonator in (a) can be mapped to an effective atom. The configuration of the multiple resonators, each now with a single effective atom, is further mapped to an effective system consisting of a single resonator and a single atom.

II. THEORETICAL MODEL

Fig. 1(a) plots the wQED architecture studied in this article. The basic configuration consists of multiple atoms evanescently couple to a WGM resonator. The next iteration is the cascade of the basic configurations to form a distributed resonator system. As an example, in Fig. 1(a), a 2-resonator configuration is illustrated in the gray-lined rectangle. The resonators couple to an optical waveguide with a separation so that the inter-resonator coupling can be neglected. The Hamiltonian describing the system in Fig. 1(a) can be written as [25]

$$\begin{aligned}\frac{H}{\hbar} =& \int dx \left(-iv_g c_R^\dagger(x)\frac{\partial}{\partial x}c_R(x) + iv_g c_L^\dagger(x)\frac{\partial}{\partial x}c_L(x)\right) \\ &+ \sum_{m=1}^{M}\left\{\sum_{n=1}^{N_m}[(\Omega_e - i\gamma)\sigma_{mn}^+\sigma_{mn}^- + \Omega_g\sigma_{mn}^-\sigma_{mn}^+]\right. \\ &+ (\Omega_r - i\gamma_r)(a_m^\dagger a_m + b_m^\dagger b_m) + (h_m a_m b_m^\dagger + H.C.) \\ &+ \int dx\delta(x - x_m)V\left(c_R^\dagger(x)a_m + c_L^\dagger(x)b_m + H.C.\right) \\ &\left.+ \sum_{n=1}^{N_m}(g_{amn}\sigma_{mn}^+ a_m + g_{bmn}\sigma_{mn}^+ b_m + H.C.)\right\}. \end{aligned} \quad (1)$$

$c_R^\dagger(x)$ ($c_R(x)$) is the creation (annihilation) operator of a waveguided right-propagating photon at x, and $c_L^\dagger(x)$ ($c_L(x)$) is similarly defined for the left-propagating photon. M is the number of resonators, each of which couples to the waveguide at x_m ($m = 1, 2, 3, ...M$), and

a number of N_m atoms couple to the m-th resonator. $\sigma_{mn}^{+(-)}$ is the raising (lowering) ladder operator of the n-th atom coupling to the mth resonator. $\hbar\Omega_e$ and $\hbar\Omega_g$ are the energies of the excited and ground state of the atom, respectively. In the excitation frequencies of atoms and resonator modes, renormalized imaginary damping terms γ and γ_r are added to characterize their interaction with the ambient environment [26, 27]. A validation of such renormalized Hamiltonian approach and a comprehensive comparison between it and other commonly used techniques has been clarified in Ref. [28]. In literature, many fruitful approaches such as Lindblad superoperator, quantum Langevin approach and quantum jumps have been widely used in describing the quantum noise and dissipations. However in these approaches, the dissipations and noises are incorporated in the system's equation of motion by a phenomenological term describing the stochastic interaction between the system and the environment, and the system-environment entanglement is inherently not taken into full consideration. Also, for those calculations of dissipations and noises based on the density matrix approach, the description is fundamentally incoherent and generates mixed state results. In contrast, renormalized decay rates in the excitation frequencies can readily preserve both the system-environment entanglement and the intra-system entanglement throughout the calculation, giving a coherent pure-state description of the system with a precision up to an arbitrarily high order. Therefore, introducing non-Hermitian decay rates in the Hamiltonian is advantageous in compactly calculating pure state solutions and predicting non-trivial phenomenon of open quantum systems in a mathematically exact manner. $\Omega \equiv \Omega_e - \Omega_g$ is the transition frequency. Ω_r is the resonance frequency of the resonator. a and b are the annihilation operators of the counter-clockwise and clockwise mode of the resonator. Within the atom cluster coupling to the m-th resonator, the n-atom ($1 \leq n \leq N_m$) in the cluster couples to the two WGMs of the resonator with a coupling $g_{amn} = |g_a|e^{i\xi\theta_{mn}}$ and $g_{bmn} = |g_b|e^{-i\xi\theta_{mn}}$ respectively, where ξ is the order number of WGM and θ_{mn} is the angular position of the atom [29]. V is the resonator-waveguide coupling strength and $\Gamma \equiv V^2/v_g$ is the resonator decay rate to the waveguide. h_m characterizes the two WGMs conversion strength (backscattering) of the m-th resonator [29]. The general

form of the system eigenstates in the single-photon regime is

$$|\Psi_\omega\rangle = \Big\{ \int dx \phi_{R,\omega}(x) c_R^\dagger(x) + \int dx \phi_{L,\omega}(x) c_L^\dagger(x) + \sum_{m=1}^{M} (\alpha_{m,\omega} a_m^\dagger + \beta_{m,\omega} b_m^\dagger) + \sum_{m=1}^{M} \sum_{n=1}^{N_m} e_{mn,\omega} \sigma_{mn}^+ \Big\} |0, -\rangle, \tag{2}$$

where $\hbar\omega$ is the energy of the photon, and $E_\omega = \hbar(\omega + \sum_{m=1}^{M} N_m \Omega_g)$ gives the energy of the eigenstate. $\phi_{R,\omega}(x)$ and $\phi_{L,\omega}(x)$ are the right and left propagating eigen-wavefunction. $\alpha_{m,\omega}$, $\beta_{m,\omega}$ and $e_{mn,\omega}$ denote the excitation amplitude of two resonator modes and the atoms respectively. $|0, -\rangle$ denotes the vacuum state containing zero photons in the waveguide with resonator modes not excited and all atoms at the ground state.

III. SUPERRADIANCE IN N ATOMS COUPLED TO ONE WGM RESONATOR

N atoms couple to one WGM resonator: We seek to establish an effective mapping (superradiance condition) so that the optical response of the configuration is identical to that of a single effective atom coupling to the resonator, for the same single-photon input. Also, the excitation amplitude and the entanglement information of the N atoms should be preserved by the effective atom throughout the interaction. For this purpose, we expand the quantum states of both systems as follows

$$|\Psi(t)\rangle = \int \frac{d\omega}{2\pi} e^{-i(\omega + N\Omega_g)t} |\Psi_\omega\rangle\langle\Psi_\omega|\Psi(0)\rangle, \tag{3a}$$

$$|\overline{\Psi}(t)\rangle = \int \frac{d\omega}{2\pi} e^{-i(\omega + \overline{\Omega}_g)t} |\overline{\Psi}_\omega\rangle\langle\overline{\Psi}_\omega|\overline{\Psi}(0)\rangle, \tag{3b}$$

where $|\Psi(t)\rangle$ denotes the state of the fundamental configuration at arbitrary time t, and the overline denotes the physical quantities pertinent to the effective system. The properties of the ground states of both systems are specified by $|\overline{-}\rangle \equiv |-\rangle$ and $\overline{\Omega}_g \equiv N\Omega_g$. For the initial condition of a left-incident single photon, the photonic eigen wavefunctions takes the form $\phi_{R,\omega}(x) = [\theta(x_1 - x) + t_\omega \theta(x - x_1)] e^{i\omega x/v_g}$ and $\phi_{L,\omega}(x) = r_\omega \theta(x_1 - x) e^{-i\omega x/v_g}$ [30] (the effective system has the same form but not shown), and the projection $\langle\Psi_\omega|\Psi(0)\rangle = \langle\overline{\Psi}_\omega|\overline{\Psi}(0)\rangle = \int dx \phi_R(x, t = 0) e^{-i\omega x/v_g}$. The expansion in Eqs. 3 reduces to $t_\omega = \overline{t}_\omega$ and $r_\omega = \overline{r}_\omega$. The preserved excitation and entanglement of atoms require $\sum_{n=1}^{N} e_{n\omega} \sigma_n^+ = \overline{e}_\omega \overline{\sigma}^+$, where $\overline{\sigma}^+$

describes the single excitation of the collectivity among the atoms (subscript "m"=1 for the resonator number is dropped). By solving $H|\Psi_\omega\rangle = E_\omega|\Psi_\omega\rangle$ and $\overline{H}|\overline{\Psi}_\omega\rangle = \overline{E}_\omega|\overline{\Psi}_\omega\rangle$, one obtains

$$t_\omega = \frac{\Delta^2\delta + \frac{\Gamma^2\delta}{4} - \Delta G_+^2 - i\frac{\Gamma G_-^2}{2} - I_1 + \frac{I_2}{\delta} - |h|^2\delta}{(\Delta + i\frac{\Gamma}{2})(\Delta\delta - G_+^2 + i\frac{\Gamma\delta}{2}) - |h|^2\delta + \frac{I_2}{\delta} - I_1} \tag{4a}$$

$$\overline{t}_\omega = \frac{\Delta^2\overline{\delta} + \frac{\Gamma^2\overline{\delta}}{4} - \Delta\overline{G}_+^2 - i\frac{\Gamma\overline{G}_-^2}{2} - \overline{I}_1 - |h|^2\overline{\delta}}{(\Delta + i\frac{\Gamma}{2})(\Delta\overline{\delta} - \overline{G}_+^2 + i\frac{\Gamma\overline{\delta}}{2}) - |h|^2\overline{\delta} - \overline{I}_1} \tag{4b}$$

where $\Delta \equiv \omega - \Omega_r + i\gamma_r$, $\delta \equiv \omega - \Omega + i\gamma$, $G_+^2 = \sum_{n=1}^N(|g_{an}|^2 + |g_{bn}|^2)$, $G_-^2 = \sum_{n=1}^N(|g_{an}|^2 - |g_{bn}|^2)$, $I_1 = \sum_{n=1}^N(g_{an}^* g_{bn} h + g_{an} g_{bn}^* h^*)$ and $I_2 = \sum_{n=1}^N \sum_{j=1}^N[|g_{an}|^2|g_{bj}|^2 - (g_{an}^* g_{bn})(g_{aj} g_{bj}^*)]$. For the effective system, $\overline{\delta} = \omega - \overline{\Omega} + i\overline{\gamma}$, $\overline{G}_+^2 = |\overline{g}_a|^2 + |\overline{g}_b|^2$, $\overline{G}_-^2 = |\overline{g}_a|^2 - |\overline{g}_b|^2$, and $\overline{I}_1 = \overline{g}_a^* \overline{g}_b h + \overline{g}_a \overline{g}_b^* h^*$. r_ω ($\overline{r}_\omega$) and $e_{n\omega}$ ($\overline{e}_\omega$) can also be obtained similarly (not shown). By equating $t_\omega = \overline{t}_\omega$, $r_\omega = \overline{r}_\omega$, and $\sum_{n=1}^N e_{n\omega}\sigma_n^+ = \overline{e}_\omega \overline{\sigma}^+$, superradiance condition is equivalent to the followng set of equalities

$$\frac{|g_{an}|}{|g_{bn}|} = \frac{|\overline{g}_a|}{|\overline{g}_b|}, \quad \forall n \tag{5a}$$

$$\xi(\theta_n - \overline{\theta}) = C\pi, \quad \forall n, (C \text{ is integer}) \tag{5b}$$

$$|\overline{g}_{a(b)}|^2 = \sum_{n=1}^N |g_{an(bn)}|^2, \tag{5c}$$

$$\overline{\Omega} - i\overline{\gamma} = \Omega - i\gamma, \tag{5d}$$

$$\overline{\sigma}^+|0,-\rangle = \sum_{n=1}^N \frac{g_{an}}{\overline{g}_a}\sigma_n^+|0,-\rangle. \tag{5e}$$

The first one and the third one set constraints on the atom-resonator couplings; while the second one indicates that the angular distance of any two atoms must be an integral multiple of π. The fourth one specifies the properties (transition frequency and the dissipation rate) of the effective atom; while the last one describes the excited state of the effective atom. We note that although the superradiance conditions in Eqs. 5 are derived for the case with an incident photon, it can be shown straightforwardly by applying time-reversal symmetry argument that they also described the time-reversed process, i.e., the cooperative single-photon emission of atoms. Thus the entangled state given by Eq. 5e is also the single-photon superradiant state that gives the maximum spontaneous emission rate.

Numerical results: To validate the single-photon superradiance effective mapping, we also carry out a rigorous numerical investigation of the system dynamics by solving the

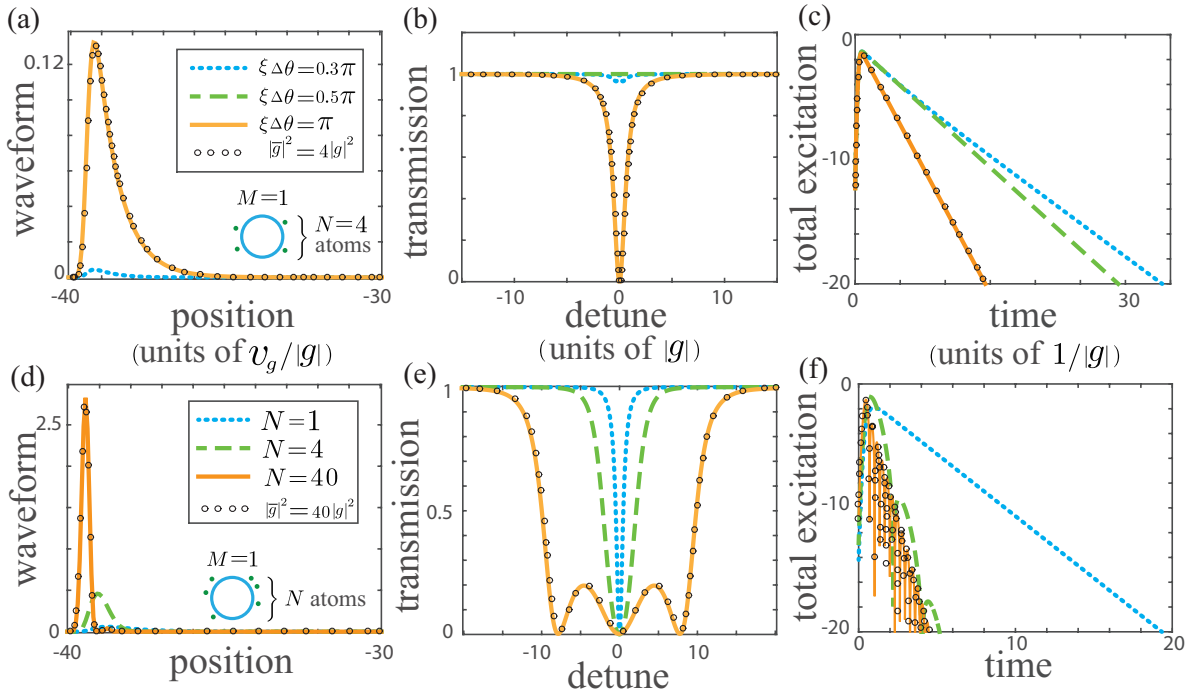

FIG. 2. (a) Reflected single-photon waveform for various atomic angular distance. The case of one effective atom with 2 times coupling ($4|g|^2$, open circle) is also shown for comparison. $\Gamma/|g| = 25$. γ_r, γ, and h are negligible. (b) Transmission spectrum for cases in (a). (c) Total atomic excitation (in log scale) for cases in (a). (d) Reflected waveform for $N = 1$ (blue/dot), 4 (green/dash), 40 (orange/solid), and the case of an effective atom with $|\overline{g}|^2 = 40|g|^2$ (open circle), when $\xi(\theta_n - \theta_{n-1}) = \pi$. $\Gamma/|g| = 9$. γ_r, γ, and h are negligible. (e) Transmission spectrum for cases in (d). (f) Total atomic excitation (in log scale) for cases in (d).

Schrödinger equation $i\hbar\partial_t|\Psi(t)\rangle = H|\Psi(t)\rangle$ numerically, using none of the assumptions in the aforementioned analytical approach. A single photon is injected into the waveguide from the far left and propagates toward to the right. The equations of motion are evolved numerically in time to trace out the full spatiotemporal dynamics of the scattering process [31]. The atoms are set to couple with two WGMs with the same strength $|g_{an}| = |g_{bn}| = |g|$ and the incident photon has a Gaussian waveform with a spatial standard deviation $\sigma = 0.1v_g/|g|$. The photon, resonator and atoms are all on resonance. Fig. 2(a)-(c) plot the case for $N = 4$ atoms with various atomic angular distance for $\Gamma = 25|g|$. For atoms with an angular distance $\xi\Delta\theta = \pi$ (orange solid curves), the system satisfies the superradiance condition and we find numerically that the optical response of the effective system is exactly the same as that

of a single atom with a coupling $|\overline{g}| = \sqrt{4}|g|$ (open circles). The reflected wave (Fig. 2(a)) exhibits a peak and then decays exponentially with a rate of $1.3|g|$. The transmission spectrum (Fig. 2(b)) follows a Lorentzian shape with a total reflection at resonance point and a full width at half maximum (FWHM) of $1.3|g|$, same as the waveform decay rate. The collective excitation of atoms $\sum_{n=1}^{N} |e_n(t)|^2$ (Fig. 2(c)) decays exponentially at a fixed rate also equivalent to $1.3|g|$ after absorbing the photon. However, when the angular distance is changed to 0.3π (blue dot curves) and 0.5π (green dash curves), where coherent interaction is broken and the superradiance condition is not satisfied, the dynamics is entirely different with the effective atom case. The reflected wave now is weak or even eliminated, with the exponential decay rate of the reflected waveform decreased to $0.5|g|$ (0.3π angular distance) and 0 (no reflection for 0.5π angular distance). The transmission spectra do not show a Lorentzian dip and photons merely get reflected due to the strong destructive interference. Also, the collective excitations of atoms decay at a much slower rate of $0.5|g|$ (0.3π angular distance) and $0.7|g|$ (0.5π angular distance).

Fig. 2(d)-(f) show the enhancement of single-photon spontaneous emission rate when the atom number N increases from 1 to 40 under the superradiance condition for $\Gamma = 9|g|$ (all other parameters are unchanged). As N increases from 1 (blue dot curves) to 4 (green dash curves) to 40 (orange solid curves), the peak in the reflected single-photon waveform becomes increasingly more prominent (Fig. 2(d)), with exponential decay rate increased from $0.9|g|$ to $4.2|g|$ to $5.7|g|$, respectively. The transmission spectrum is broadened (Fig. 2(e)) with the FWHM of the transmission spectrum broadened from $0.9|g|$ ($N = 1$) to $4.3|g|$ ($N = 4$), and it is even split to three dips for $N = 40$. The collective atomic excitation (Fig. 2(f)) also decays at a faster rate, from $0.9|g|$ ($N = 1$) to $4.5|g|$ ($N = 4$) to $5|g|$ ($N = 40$). Interestingly, for the $N = 4$ case, the collective atom excitation in Fig. 2(f) exhibits a transient oscillation pattern which has a linear decay envelope in the semi-log plot. The transient oscillation becomes more rapidly when N increases to 40. As N increases, the coupling strength crossovers from weak-coupling regime $\Gamma \gg \sqrt{N}|g|$ for $N = 1$ to the strong-coupling regime $\Gamma \simeq \sqrt{N}|g|$ for $N = 4$ and 40 (which can be achieved even for small $|g|$). Consequently, the small photonic relaxing rate Γ from the resonator to the waveguide in the strong-coupling regime presents a bottleneck for photon transfer, and accordingly the photon would jump coherently between the resonator and the atoms numerous times before it is eventually leaked to the waveguide, resulting in such an oscillation of atomic excitation.

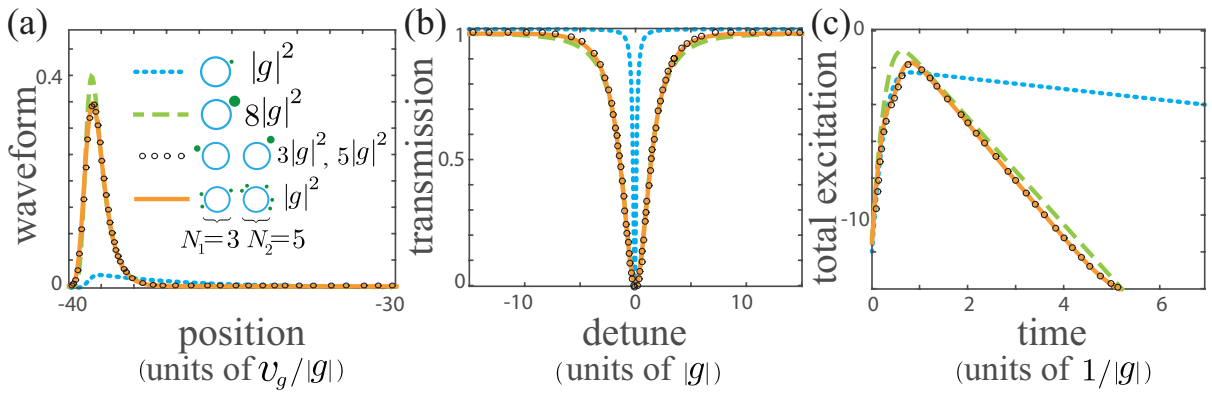

FIG. 3. (a) Reflected waveform of a short Gaussian wavepacket input. Orange solid curve: $N_1 = 3$, $N_2 = 5$, and the cascade system satisfies the superradiance condition. Open circle: the atoms on each resonator are replaced by one effective atoms ($|\overline{g}_1|^2 = 3|g|^2$, $|\overline{g}_2|^2 = 5|g|^2$). Green dash curve: the cascade system is replaced by a renormalized atom (coupling strength $|\overline{g}^R|^2 = 8|g|^2$) coupled to one WGM resonator. Blue dot curve: a comparison case that a single atom (coupling strength $|g|$) couples to a resonator. $\Gamma/|g| = 25$. γ_r, γ, and h are negligible. (b) Transmission spectrum. (c) Total atomic excitation (in log scale).

In the strong-coupling regime, the atomic decay rate does not increase further when N is increased, as the rate is fundamentally limited by Γ. Nonetheless, the optical responses of $N = 40$ case and effective atom with $|\overline{g}|^2 = 40|g|^2$ (open circles) (Fig. 2(d)) remain identical.

In the weak coupling regime, where cooperative atom number is small and $|\overline{g}|^2 \ll \Gamma^2$, the transmission spectrum can be well approximated by a Lorentzian shape with FWHM $8|\overline{g}|^2/\Gamma$, and the collective spontaneous decay rate of atoms scales linearly with atom number N. When the number of cooperative atoms increases so that $8|\overline{g}|^2 > \Gamma^2$, the bottleneck effect comes into play. The linear scaling of atomic decay rate fails, and the transmission spectrum will split into three dips, with two off resonance total reflection dips at $\omega = \Omega \pm \sqrt{2|\overline{g}|^2 - \Gamma^2/4}$. By further increasing superradiant coupling strength to the strong coupling regime $|\overline{g}|^2 \gg \Gamma^2$, the FWHM of the center dip in the transmission spectrum and the general decay rate of atoms both gradually approaches Γ as $|\overline{g}| \to \infty$.

IV. SUPERRADIANCE IN CASCADED WGM RESONATORS

Cascaded WGM resonators: A solid-state WGM resonator typically has a size of order 10∼100 μm, thus a photon wavepacket (usually has a spatial size > 1 mm) can couple coherently to multiple resonators at the same time, indicating the possibility of single-photon superradiance for cascaded systems. Our strategy for investigating the single-photon superradiance phenomenon in a multi-atom multi-resonator configuration is through a renormalization process (Fig. 1(b)): first, the atoms coupled to each resonator is mapped to an effective atom via the aforementioned single-resonator superradiance condition; next, the configuration of the multiple resonators, each now is coupled with only a single effective atom, is further mapped to an effective system consisting of one renormalized single resonator and one renormalized single atom that exhibits the single-photon superradiance. To illustrate the process, we consider a two-resonator case, wherein each resonator couples to an effective atom with coupling strength $\overline{g}_{a1}$, $\overline{g}_{b1}$ and $\overline{g}_{a2}$, $\overline{g}_{b2}$, respectively. To describe the cascade system's superradiance in the effective mapping picture, we search for the conditions when the transport property of the two-resonator cascade (described by $\overline{t}_{\omega}^{(2)}$ and $\overline{r}_{\omega}^{(2)}$) are physically equivalent to that of a renormalized one-atom one-resonator effective system (described by $\overline{t}_{\omega}^{R}$ and $\overline{r}_{\omega}^{R}$; the superscript R denotes the renormalized single-resonator system), *i.e.*, $|\overline{t}_{\omega}^{(2)}|^2 = |\overline{t}_{\omega}^{R}|^2$ and $|\overline{r}_{\omega}^{(2)}|^2 = |\overline{r}_{\omega}^{R}|^2$. Due to the accumulated phase retardation of the running waves propagating within multiple resonators, here we require only the equality of the norm of the amplitude but not the phase. After some algebra, the two systems are found to be physically equivalent under the following set of conditions: (1) The distance between the resonators is an integer multiple of $\lambda/2$ (λ is the wavelength corresponding to photon center frequency); (2) The resonators are identical, and are on resonance with the atoms $\Omega_r = \overline{\Omega} = \Omega$; (3) The atoms couple to two counter-propagating modes with the same strength $|\overline{g}_{a1,2}| = |\overline{g}_{b1,2}| = |\overline{g}_{1,2}|$, and atom-resonator coupling is much weaker than resonator-waveguide coupling $\Gamma^2 \gg 2|\overline{g}_1|^2 + 2|\overline{g}_2|^2$; (4) The angular positions of two effective atoms satisfy $\xi(\overline{\theta}_1 - \overline{\theta}_2) = C\pi$ (C is integer); and (5) The back-scattering strength $|h_{1,2}|$ and dissipations γ_r, γ are all negligible compared to $|\overline{g}_{1,2}|$. These sufficient conditions leads to $|\overline{t}_{\omega}^{(2)}|^2 \approx |\overline{t}_{\omega}^{R}|^2$ with renormalized effective parameters $\overline{\Omega}_r^R = \Omega_r$, $\overline{\Gamma}^R = \Gamma$ and $|\overline{g}^R| = \sqrt{|\overline{g}_1|^2 + |\overline{g}_2|^2}$. That is, the two-resonator cascade now can be mapped to a renormalized one-atom one-resonator effective system, wherein the renormalized resonator has ex-

actly the same properties as those in the original two-resonator system but the renormalized resonator-atom coupling is enhanced. The superradiance condition can be straightforwardly generalized to a multi-resonator cascade, wherein the renormalized superradiant coupling strength is $|\overline{g}^R| = \sqrt{\sum_{m=1}^{M}\sum_{n=1}^{N_m}|g_{mn}|^2}$.

Numerical results: For the two-resonator case, each resonator is coupled with a number of identical atoms ($N_1 = 3$ and $N_2 = 5$, respectively; $|g_a| = |g_b| = |g|$ for each atom; and $\Gamma/|g| = 25$). The incident photon pulse has a width $\sigma = 0.1v_g/|g|$ and all parameters are set to satisfy the superradiance condition. The results are shown in Fig. 3. Compared with the one-atom one-resonator case with an atom-resonator coupling strength $|g|$ (blue dot curve), the cascade system (orange solid curve) exhibits a prominent reflection peak (Fig. 3(a)), a broadened transmission spectrum (Fig. 3(b)), and an enhanced collective atomic excitation decay rate (Fig. 3(c)), which are all signatures of single-photon superradiance. Also shown in Fig. 3 (open circles) is the case wherein the atoms coupled with each resonator are replaced by one effective atom (with $|\overline{g}_1|^2 = 3|g|^2$ and $|\overline{g}_2|^2 = 5|g|^2$ respectively). The agreement with the cascade system (orange solid curve) provides a numerical support for the equivalence of the two systems, as established previously. Moreover, the numerical results for a renormalized system (a renormalized atom with $|\overline{g}^R|^2 = 8|g|^2$ coupled to a renormalized resonator with $\overline{\Gamma}^R = \Gamma$), as shown by the green dash curves, indicate that single-photon superradiance for the multi-atom two-resonator cascade system can be well-approximated by a renormalized one-atom one-resonator system. Quantitatively, the decay rate of the emitted waveform, the decay rate of the total atomic excitation, and the bandwidth of the transmission spectrum share a same value of $2.88|g|$ for both the renormalized system (green dash curve) and the cascaded system (open circles), while the single atom case (blue dot curve) has a value of $0.35|g|$. We note that there exists a linear scaling in decay rate approximately proportional to atom number N since the system is still in weak coupling regime.

V. SINGLE PHOTON FREQUENCY COMB GENERATION

The enhanced interaction between atoms and a single-photon under superradiance conditions can be exploited to distinguish nontrivial optical phenomena that are otherwise subtle for feeble atom-photon interactions. Here we describe the generation of single-photon frequency comb via a slowly frequency-modulated superradiant effective atom with a chiral

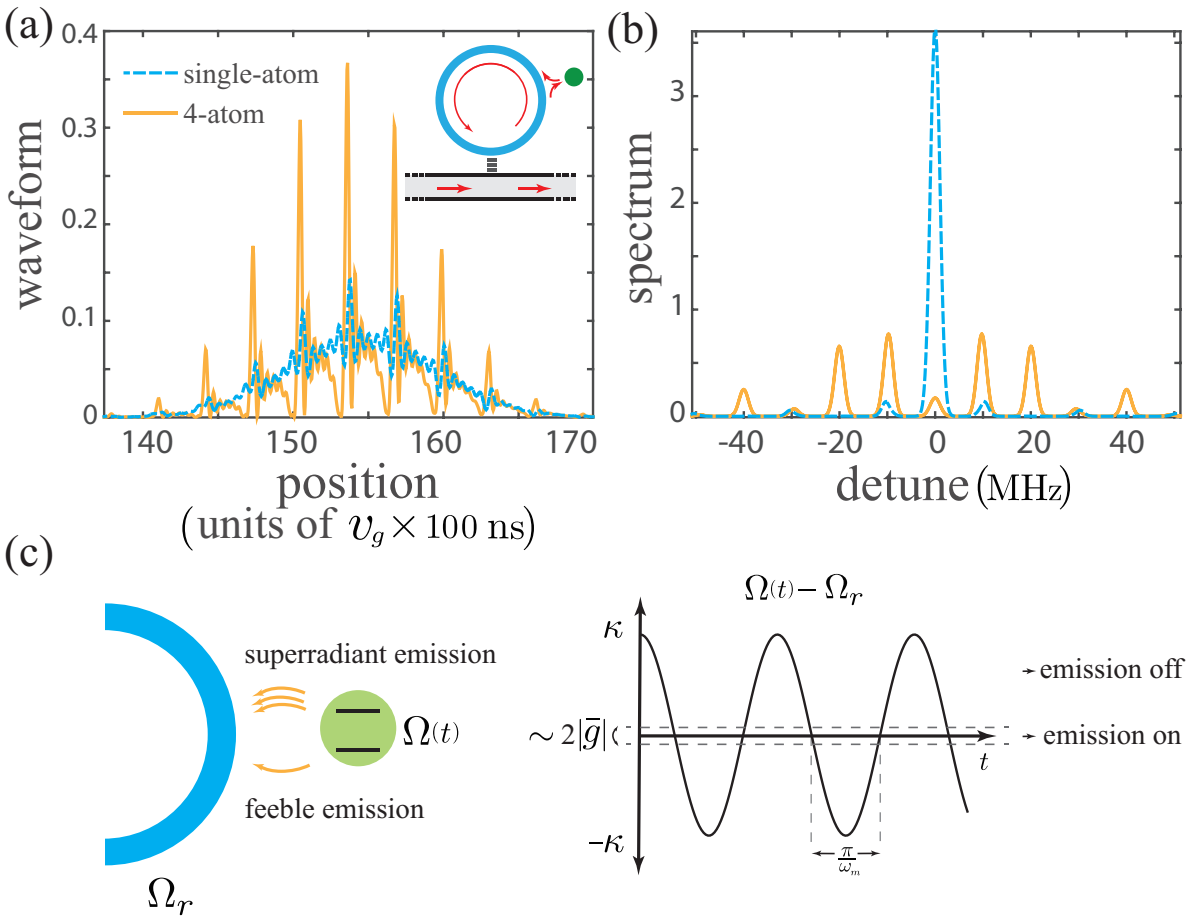

FIG. 4. Single-photon frequency comb generation. (a) Inset: Schematics. A frequency-modulated effective superradiant atom (green dot) chirally couples to the counter-clockwise mode of a WGM resonator. Transmitted single-photon wavepacket for a single atom ($N = 1$, blue dash curve) and for superradiant atom consisting of four atoms ($N = 4$, orange solid curve), respectively. The input photon has a long Gaussian waveform. (b) The frequency spectra of the output wavepforms in (a). (c) Physical picture of an effective atom coupled to a resonator and the modulation of atom transition frequency. The effective coupling strength determines both the rate of spontaneous emission and the bandwidth of coupling ($\sim 2|\overline{g}|$). The spontaneous emission occurs only when the atom transition frequency is near resonance inside the coupling bandwidth.

coupling [32]. A single-photon frequency comb is an optical spectrum of a single-photon pulse which consists of equidistant spectral lines over a wide bandwidth [33, 34]. Single-photon frequency comb is an important tool for high-precision optical metrology and also provides a means for encoding qubits in quantum communication. Although a number of

frequency comb generation schemes exist, to date it is still challenging to generate frequency combs at single-photon levels. Here we present a generation method based on strong atom-light coupling in WGM resonators. The configuration is schematically plotted in the inset of Fig. 4(a): an effective atom (green dot), which represents a cluster of atoms under the aforementioned superradiance condition, asymmetrically couples to only one of the two WGMs of the resonator (counter-clockwise mode in this case), where the transition frequency of the atoms is modulated by a slowly-changing external electric field. One effect of the external modulation is the nonlinear frequency mixing between that of the single-photon and the modulation frequency, in order to generate sideband components desired in a frequency comb. The chiral coupling can be created by using strong light confinement to lock the local polarization of the light to its propagation direction at the emitters [32]. As a result, even though both counter-propagating WGMs are supported in the resonator, the quantum emitters preferentially couple to light unidirectionally. With the couplings taken directly from a recent experiment for a chiral waveguide QED system [35], the waveguide-resonator coupling strength Γ is assumed to be 40 MHz, and each atom couples to the resonator with a strength $|g_a| = 24$ MHz ($|g_b| = 0$ Hz due to the chiral coupling). The atoms are modulated by a slowly-varying external electric field with a frequency $\omega_m = 10$ MHz, which is small compared to the typical atom transition frequency ($\gg 1$ THz in [35]). Via the Stark effect, the transition frequency of the atoms now changes with time and becomes $\Omega(t) = \Omega + \kappa\cos(\omega_m t)$, where the modulation amplitude κ is chosen to be 300 MHz [36]. Consider a long single-photon Gaussian wavepacket with a spatial width $\sigma = v_g \times 500$ ns incident from the left port of the waveguide. After interacting chirally with the frequency-modulated superradiant atom, the photon is scattered unidirectionally to the right output port of the waveguide. Fig. 4(a) plots the output waveform for the case when the effective atom consists of four atoms (orange solid curve). Instead of a single superradiant peak, the modulation now gives rise to a series of narrow and strong superradiant peaks. Accordingly, in the frequency domain, as shown in Fig. 4(b) (orange solid curve), the modulation of the superradiant effective atom enables efficient conversion and redistribution of the photon energy into equidistant sidebands centered at $\Omega \pm l\omega_m, l = 1, 2, 3, ...$, respectively, exhibiting a single-photon frequency comb. The center frequency peak is largely suppressed so that the output photon is mostly off-resonant to the superradiant effective atom. Also, by eliminating the far-detune frequency components with proper optical bandpass filters, the fast

oscillation noises in the wavepacket can be suppressed. As a comparison, in Fig. 4(a), we also show the output waveform for the modulated single-atom case (blue dash curve), wherein the modulation merely induces small-amplitude ripples superimposed on the single-photon Gaussian profile. The modulation also causes weak sideband components in the frequency spectrum, but most of the photon energy remains in the original bandwidth, as shown by the strong center peak in Fig. 4(b) (blue dash curve). A physical picture of how frequency comb is improved by superradiant coupling is depicted in Fig. 4(c). As the external electrical field drives the transition frequency of the atoms to change sinusoidally between $\Omega + \kappa$ and $\Omega - \kappa$, the atom-resonator energy exchange is turned on and off periodically since it only occurs when atoms are near resonance with the resonator (within the atom coupling bandwidth $\sim 2|\overline{g}|$). Consequently, spontaneous emission peaks are imposed on the photon wavepacket periodically and creates comb shaped equal-distant peaks in both space and frequency domain. The distances between individual peaks are $\pi v_g/\omega_m$ and ω_m in the space and frequency domain, respectively. Each peak in the frequency domain follows the shape and the FWHM with the initial input wavepacket. Since the effective coupling strength $|\overline{g}|$ characterizes the rate of spontaneous emission, a stronger coupling results in more sharpened peaks and correspondingly more high frequency components in the spectrum, i.e., better frequency comb quality. However, an exceedingly high coupling strength does not generate an ideal frequency comb, as the broad coupling bandwidth ($2|\overline{g}| \sim \kappa$) of the atoms will preserve the resonator-atom coupling for most of time and degrades the periodic on/off modulation to the atomic spontaneous emission. Under that situation, the physical picture is similar to a photon coupled to atoms that are subject to a phonon mode, resulting in only two Stocks and anti-Stocks sidebands at $\Omega - \omega_m$ and $\Omega + \omega_m$ in the output photon spectrum, respectively.

VI. CONCLUSION

In this article, we present an effective mapping method to investigate single-photon superradiance for whispering-gallery-mode resonator systems in wQED systems. Such an effective mapping is a wavefunction based first principle method that focus on the fundamental physics of cooperative atom-light interaction. The occurrence conditions for single-photon superradiance in WGM systems are rigorously derived and the specific entanglement of

atoms that gives the maximum superradiant spontaneous emission rate is uncovered. Furthermore, as our method maintains the coherence between atoms and the photon wavefunction, it provides a comprehensive picture of the changed photon scattering properties under superradiance such as peaked emission intensity, broadened transmission spectrum and oscillating resonator-atom energy exchange due to the bottlenecked resonator coupling, to a high quantitative accuracy.

Our results provide a basis for potential applications of single-photon superradiance in the atoms-WGM resonator systems. By exploiting the ultra-strong coupling strength in a superradiant atoms-WGM resonator system, nontrivial optical responses can be engineered, as what we have presented in the generation of single-photon frequency comb. Also, the manipulation of the effective coupling strength is potentially useful in efficient photon routing in quantum circuits [35]. Furthermore, the entangled Dicke state maintained in a superradiant atoms-WGM resonator system allows the control of phase coherence and synchronization of dynamics between distant particles [37], which are the essential ingredients for large-scale quantum information systems. Finally, as multi-photon nonlinearity is essential in various fields, it would be of great importance to extend and generalize our approach for investigating multi-photon superradiance for generating novel and strong nonlinear quantum optical properties.

ACKNOWLEDGMENTS

This work was supported in part by NSF ECCS Grant No. 1608049 and No. 1838996.

[1] R. H. Dicke, Phys. Rev. **93**, 99 (1954).

[2] M. Gross and S. Haroche, Physics Reports **93**, 301 (1982).

[3] R. Rhlsberger, K. Schlage, B. Sahoo, S. Couet, and R. Rffer, Science **328**, 1248 (2010).

[4] R. Friedberg and J. T. Manassah, Physics Letters A **374**, 1648 (2010).

[5] D. E. Chang, L. Jiang, A. V. Gorshkov, and H. J. Kimble, New Journal of Physics **14**, 063003 (2012).

[6] M. O. Scully, E. S. Fry, C. H. R. Ooi, and K. Wdkiewicz, Phys. Rev. Lett. **96**, 010501 (2006).

[7] M. O. Scully, Phys. Rev. Lett. **115**, 243602 (2015).

[8] L.-M. Duan, M. D. Lukin, J. I. Cirac, and P. Zoller, Nature **414**, 413 EP (2001).

[9] A. A. Svidzinsky, F. Li, H. Li, X. Zhang, C. H. R. Ooi, and M. O. Scully, Phys. Rev. A **93**, 043830 (2016).

[10] Z. Liao, H. Nha, and M. S. Zubairy, Phys. Rev. A **94**, 053842 (2016).

[11] K. Lalumire, B. C. Sanders, A. F. van Loo, A. Fedorov, A. Wallraff, and A. Blais, Phys. Rev. A **88**, 043806 (2013).

[12] A. Goban, C.-L. Hung, J. D. Hood, S.-P. Yu, J. A. Muniz, O. Painter, and H. J. Kimble, Phys. Rev. Lett. **115**, 063601 (2015).

[13] A. Asenjo-Garcia, M. Moreno-Cardoner, A. Albrecht, H. J. Kimble, and D. E. Chang, Phys. Rev. X **7**, 031024 (2017).

[14] J. S. Douglas, H. Habibian, C.-L. Hung, A. V. Gorshkov, H. J. Kimble, and D. E. Chang, Nature Photonics **9**, 326 EP (2015).

[15] K. J. Vahala, Nature **424**, 839 EP (2003).

[16] A. Yariv, Electronics Letters **36**, 321 (2000).

[17] L. Maleki, A. B. Matsko, A. A. Savchenkov, and V. S. Ilchenko, Opt. Lett. **29**, 626 (2004).

[18] J. E. Heebner, R. W. Boyd, and Q.-H. Park, Phys. Rev. E **65**, 036619 (2002).

[19] F. Vollmer and S. Arnold, Nature Methods **5**, 591 EP (2008).

[20] Y. Shen, D.-R. Chen, and J.-T. Shen, Phys. Rev. A **85**, 063808 (2012).

[21] J. W. Silverstone, R. Santagati, D. Bonneau, M. J. Strain, M. Sorel, J. L. O'Brien, and M. G. Thompson, Nature Communications **6**, 7948 EP (2015).

[22] Y. Zhou, Z. Chen, and J.-T. Shen, Phys. Rev. A **95**, 043832 (2017).

[23] H. Eleuch and I. Rotter, The European Physical Journal D **68**, 74 (2014).

[24] H. Eleuch and I. Rotter, Phys. Rev. A **95**, 022117 (2017).

[25] Y. Shen and J.-T. Shen, Phys. Rev. A **85**, 013801 (2012).

[26] Z. Chen, Y. Zhou, and J.-T. Shen, Opt. Lett. **42**, 887 (2017).

[27] Z. Chen, Y. Zhou, and J.-T. Shen, Phys. Rev. A **96**, 053805 (2017).

[28] Z. Chen, Y. Zhou, and J.-T. Shen, Phys. Rev. A **98**, 053830 (2018).

[29] J.-T. Shen and S. Fan, Phys. Rev. A **79**, 023838 (2009).

[30] J. T. Shen and S. Fan, Opt. Lett. **30**, 2001 (2005).

[31] M. Bradford and J.-T. Shen, Phys. Rev. A **85**, 043814 (2012).

[32] P. Lodahl, S. Mahmoodian, S. Stobbe, A. Rauschenbeutel, P. Schneeweiss, J. Volz, H. Pichler,

and P. Zoller, Nature **541**, 473 EP (2017).

[33] Z. Liao, H. Nha, and M. S. Zubairy, Phys. Rev. A **93**, 033851 (2016).

[34] C. Ren and H. F. Hofmann, Phys. Rev. A **89**, 053823 (2014).

[35] S. Rosenblum, O. Bechler, I. Shomroni, Y. Lovsky, G. Guendelman, and B. Dayan, Nature Photonics **10**, 19 EP (2015).

[36] M. W. Noel, W. M. Griffith, and T. F. Gallagher, Phys. Rev. A **58**, 2265 (1998).

[37] N. Yokoshi, K. Odagiri, A. Ishikawa, and H. Ishihara, Phys. Rev. Lett. **118**, 203601 (2017).